

Improved Anthropogenic Mercury Emission Inventories for China from 1980 to 2020: Toward More Accurate Effectiveness Evaluation for the Minamata Convention

Yang Zhang, Lei Zhang,* Shuzhen Cao, Xia Liu, Jingmeng Jin, and Yu Zhao



Cite This: *Environ. Sci. Technol.* 2023, 57, 8660–8670



Read Online

ACCESS |

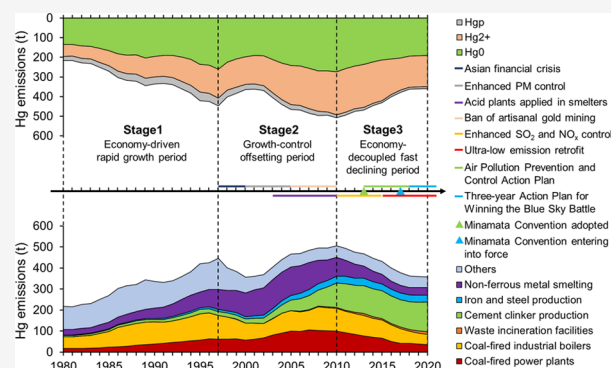
Metrics & More

Article Recommendations

Supporting Information

ABSTRACT: Anthropogenic mercury (Hg) emission inventories are crucial for the effectiveness evaluation of the Minamata Convention on Mercury. In this study, we developed an integrated Dynamic Inventory for Mercury Emission (DIME) model and improved the accuracy of emission estimates for primary sources in China. Long-term historical speciated Hg emission inventories for China were established. The total Hg emissions increased from 217.0 t in 1980 to 357.8 t in 2020 with a peak value of 506.6 t in 2010. Three stages with distinct leading drivers were identified. At Stage 1 (1980–1997), Hg emissions doubled with the rapid growth of economy; the driver was offset by the increase of dust and SO₂ control measures at Stage 2 (1997–2010) except for cement production; and co-benefits from strict control measures induced the decoupling of Hg emissions from the economy at Stage 3 (2010–2020). The ultralow emission (ULE) retrofits in key industries had pronounced Hg removal efficiencies. Large emission reduction potential still exists in the cement industry. The improved emission estimation methods for key sectors, the consistency in methodology for historical Hg emission inventories, and the more accurate spatial distribution of speciated Hg emissions in this study provide a practical toolkit for the effectiveness evaluation of the Minamata Convention.

KEYWORDS: mercury emission inventory, China, Minamata Convention, effectiveness evaluation, probabilistic model.



1. INTRODUCTION

Mercury (Hg) is a persistent, bioaccumulative, and neurotoxic global pollutant which is transported over long distances through atmospheric circulation and deposits onto the earth's surface, causing adverse effects on ecosystems and human health.¹ Mercury in the atmosphere has three operationally defined forms, namely, gaseous elemental mercury (GEM or Hg⁰), gaseous oxidized mercury (GOM or Hg²⁺), and particle-bound mercury (PBM or Hg_p).² To reduce global Hg pollution, the Minamata Convention on Mercury has entered into force with five point source categories addressed, including coal-fired power plants (CFPPs), coal-fired industrial boilers (CFIBs), non-ferrous metal smelters (NFMSs), cement clinker plants (CCPs), and waste incineration facilities (WIFs). A series of air pollution control devices (APCDs) have been installed in various industries to reduce NO_x, SO₂, and particulate matter (PM) in recent years, leading to co-benefits of atmospheric Hg emission reduction.^{3–7} As the largest anthropogenic Hg emitter, China shall establish accurate inventories of Hg emissions from key sources and evaluate the effectiveness of Hg emission control.

Hg emission inventories for the CFPP sector in China have been evolving since the beginning of this century. Streets et al.⁸ established a comprehensive emission inventory for CFPPs in

China for the year 1999 regarding coal Hg contents by province, boiler types, and APCDs with only PM control devices considered at the time. Electrostatic precipitators (ESPs) and wet flue gas desulfurization systems (WFGDs) in CFPPs were found to have co-benefits on Hg removal.⁹ Zhang et al.¹⁰ quantified the impacts of coal quality, primarily chlorine (Cl) content, on Hg speciation, transformation, and removal across APCDs, especially ESP+WFGD, and developed a coal quality-regarded probabilistic emission factor model to establish Hg emission inventory of CFPPs in China in 2008. The selective catalytic reduction (SCR) system for NO_x control was rapidly spread out in CFPPs in China during 2010–2015, which promoted the conversion of Hg⁰ to Hg²⁺ in flue gas and enhanced Hg removal in the downstream WFGD.¹¹ The implementation of the Air Pollution Prevention and Control Action Plan accelerated the development of

Received: February 8, 2023

Revised: April 20, 2023

Accepted: May 16, 2023

Published: June 1, 2023



ultralow emission (ULE) retrofits in Chinese CFPPs, including the installation of newly built advanced electrostatic fabric filters (ESP-FFs), wet electrostatic precipitators (WESPs), and low-temperature electrostatic precipitators (LTESPs), resulting in a 57 t reduction of Hg emissions during 2013–2017.⁴

NFMS was estimated to be the largest Hg emission sector in China in early studies.^{8,12} However, Hylander and Herbert¹³ found the Hg emission from this sector was largely overestimated due to the neglect of co-benefit Hg removal from acid plants in smelters. Wu et al.¹⁴ updated the Hg contents in non-ferrous metal concentrates by province based on nationwide sampling and analysis, took the co-benefit Hg removal effect by APCDs in smelters into consideration, and found a first ascending then descending trend in the NFMS sector in China during 2000–2010. Zhang et al.⁶ incorporated the Monte Carlo simulation into the emission inventory model and found the NFMS Hg emission inventory being underestimated by previous studies with the adoption of geometric means of Hg content in metal concentrates. In a recent study, Cao et al.¹⁵ unveiled a “Hg removal compensation effect” between cascaded APCDs in smelters, improved the Hg emission inventory model for the NFMS sector, and estimated a 55.6 t emission reduction from 2010 to 2017.

Around 2010, CCP began to take the lead in Hg emission among all sectors in China.^{16–18} Dust recycling in the precalciner process in cement plants could cause Hg accumulation in the kiln system and significantly limit the Hg removal efficiencies of PM control devices.^{17,19,20} Cai et al.²¹ estimated that Hg emissions from CCPs in China increased from 80 to 113 t from 2007 to 2015 based on the mass balance method and plant-level input–output data. Coal is used as fuel in cement production, but is categorized into the industrial coal combustion sector in China Energy Statistical Yearbooks which were the most commonly used sources for activity data of coal consumption.^{6,22} Therefore, previous studies^{6,8,12} tended to exclude the part of Hg emissions from coal use in cement production to avoid double counting. However, due to the low Hg removal efficiency resulting from dust recycling, the above-mentioned data source-based calculation could cause underestimation for the CCP sector in China. Another limitation was that the CFIB sector addressed by the Minamata Convention could not be separated from industrial coal combustion. A recent study assessed the Hg emissions from the CFIB sector in China based on a new data source specifically for CFIBs using a bottom-up emission factor method and made a more reliable estimation for this sector.²³

Aside from CFPP, NFMS, CCP, and CFIB, iron and steel production (ISP) was estimated to be the fifth largest Hg emission sector in China.^{6,18} Wu et al.²⁴ updated the Hg emission inventories for the ISP sector in China from 2000 to 2015 using a technology-based emission factor method and found a total emission of 32.7 t in 2015. Nevertheless, the ULE retrofits have also been applied to the ISP sector since 2019. The improved APCDs in this sector, especially the SCR systems for NO_x control, could enhance synergistic Hg removal.

Dynamic anthropogenic atmospheric Hg emission inventories for China have been developed by Wu et al.¹² (1995–2003), Zhang et al.⁶ (2000–2010), Tian et al.²⁵ (1949–2012), Huang et al.²⁶ (1980–2012), Zhao et al.²⁷ (2005–2012), Wu et al.¹⁸ (1978–2014), and Liu et al.⁴ (2013–2017). However, inventory models used in these studies were diversified, and

more advanced methods have been developed for key emission sectors in China in recent years.^{15,17,24,28,29} To keep the consistency in methodology and further improve the accuracy of Hg emission inventories, a more comprehensive inventory model was developed in this study, and anthropogenic Hg emission inventories for China for the period of 1980–2020 were established with Hg speciation included. Rapidly growing ULE measures taken in the sectors of CFPP, CFIB, CCP, and ISP in China in recent years were considered for the first time. The improved inventories could provide reliable historical trends of Hg emissions in China, toward more accurate effectiveness evaluation for the Minamata Convention.

2. METHODOLOGY

2.1. Model Description. Based on the framework of the CAME model in Zhang et al.⁶ an integrated Dynamic Inventory for Mercury Emission (DIME) model was developed in this study for estimating anthropogenic Hg emissions. All Hg emission sources in DIME were divided into 24 types and classified into four tiers, as shown in Supporting Information (SI) Table S1. The more advanced tiers incorporate more information into the estimation methods, leading to lower uncertainty levels. Tiers 3 and 4 cover the most important Hg emission sources in China (CFPP, NFMS, CFIB, CCP, and ISP), accounting for over 80% of anthropogenic Hg emissions in China.⁶ In the DIME model, Tier 4 sources, with the most advanced estimation methods, contain NFMS and CFPP, which take into consideration the impacts of the “Hg removal compensation” effect and coal quality on Hg removal efficiencies of APCDs, respectively (see details in Section 2.2). In comparison, Tier 4 in CAME⁶ only contains CFPPs equipped with ESP and ESP+WFGD. For Tier 3 sectors, the way of source classification for coal combustion was updated from administration- or statistics-based to function- or technology-based as illustrated in detail in SI Section S2. As a result, Hg emissions from CFIBs and CCPs could be estimated more accurately than the general concept “industrial coal combustion” in the previous CAME model.⁶ With the implementation of stricter environmental regulations during 2015–2020, especially the ULE retrofits, high-efficiency APCDs applied in the sectors of CFPP, CFIB, CCP, and ISP were all taken into consideration for the first time, which are further discussed in Section 2.3.3. In previous studies,^{4,5} only ULE measures in CFPPs were considered. All of the improvements above could lead to reduced uncertainties in the estimation of Hg emissions from the key sources listed in the Minamata Convention, toward more accurate effectiveness evaluation.

2.1.1. Single Emission Factor Model. Hg emissions from sources in Tier 1 with limited information were calculated by the single emission factor model, as shown in eq 1

$$E = \sum_i (EF \cdot AL_i) \quad (1)$$

where E is the total Hg emission; i is the province; EF is the emission factor, which could be either fuel/raw material-based or product-based; and AL is the corresponding activity level.

2.1.2. Deterministic Technology-Based Emission Factor Model. The model for Tier 2 sources was technology-based, which considers the production process and APCDs applied. The calculation formula is shown as eq 2

$$E = \sum_i \sum_j \left(C_i \cdot M_i \cdot \gamma_j \cdot \sum_k (P_{jk} \cdot (1 - \eta_k)) \right) \quad (2)$$

where C is the consumption of fuels or raw materials; M is the Hg content of the consumed fuels or raw materials; γ is the Hg release rate; P is the application rate of an APCD combination; η is the Hg removal efficiency of an APCD combination; j is the type of production process; and k is the type of APCD combination.

2.1.3. Probabilistic Technology-Based Emission Factor Model. From Tier 2 to 3, the model was upgraded to a probabilistic version which takes the probability distribution of key parameters into consideration. The calculation formula is shown as eq 3

$$E(\{x_i\}, \{y_k\}) = \sum_i \sum_j \left(C_i \cdot M_i(x_i) \cdot \gamma_j \cdot \sum_k (P_{jk} \cdot (1 - \eta_k(y_k))) \right) \quad (3)$$

where $E(\{x_i\}, \{y_k\})$, $M(x_i)$, and $\eta(y_k)$ are the probability distributions of E , M , and η , respectively.

2.1.4. Probabilistic Technology-Based Emission Factor Model Regarding Key Impact Factors. From Tier 3 to 4, the model integrated submodels to quantify the impacts of key factors on Hg removal efficiencies of APCDs. An example of the calculation formula for CFPP is as follows

$$E(\{x_i\}, \{z_l\}) = \sum_i \sum_j \left(C_i \cdot M_i(x_i) \cdot \gamma_j \cdot \sum_k \left(P_{jk} \cdot \prod_l (1 - \eta_{kl}(M(x), CC(z), \dots)) \right) \right) \quad (4)$$

where $E(\{x_i\}, \{z_l\})$ is the probability distribution of E ; l is the l th APCD in the k th combination; $\eta(M, CC, \dots)$ is η as a function of key factors; and $CC(z)$ is the probability distribution of coal Cl content.

2.2. Submodels for Tier 4 Sources. Tier 4 contains the sectors of NFMS and CFPP. The submodel for NFMS has been illustrated in our previous study¹⁵ with the “Hg removal compensation” effect of cascaded APCDs considered. The submodel for CFPP incorporated the impacts of coal quality, mainly Cl and Hg content, on Hg transformation and removal across APCDs. The behaviors of Hg in flue gases inside ESP and WFGD have been quantified and applied to Hg emission estimation in our previous study.¹⁰ In recent years, SCR has been more and more widely used in CFPPs in China with the application rate reaching 85% in 2015. SCR could promote the oxidation of Hg^0 to Hg^{2+} , and Hg^{2+} could be partly adsorbed onto particles and converted to Hg_p .¹ The Hg behaviors could be described as follows

$$[\text{Hg}^0]_2 = (1 - \varepsilon_o)[\text{Hg}^0]_1 \quad (5)$$

$$[\text{Hg}^{2+}]_2 = (1 - \varepsilon_a)[\text{Hg}^{2+}]_1 + \varepsilon_o[\text{Hg}^0]_1 \quad (6)$$

$$[\text{Hg}_p]_2 = [\text{Hg}_p]_1 + \varepsilon_a[\text{Hg}^{2+}]_1 \quad (7)$$

where subscripts 1 and 2 stand for the concentrations of the relevant Hg species before and after SCR, respectively; ε_o is the oxidation rate of Hg^0 ; and ε_a is the adsorption rate of Hg^{2+} .

Based on field test data from existing studies,^{30–34} a significant positive correlation between the Hg^0 concentration at the inlet of SCR and the Hg^0 oxidation rate in SCR was observed, as shown in SI Figure S1. The goodness of fit (R^2) reached as high as 0.72 ($p = 0.002$), indicating that the Hg content of coal has the most significant impact on the oxidation process inside SCR. However, the information on the Cl content of coal was not sufficient to address its impact on the process. As a result, a submodel for Hg emission calculation across the combination of SCR+ESP+WFGD was developed. More details on the submodel for CFPP can be found in SI Section S2. The Hg^{2+} adsorption rate inside SCR was fixed at 6% based on existing studies.^{30–34}

2.3. Activity Levels and Key Parameters. **2.3.1. Activity Levels.** Most information on the consumption amounts of fuels/raw materials originated from the statistical yearbooks. The amounts of provincial clinker production were derived from Liao et al.³⁵ instead of conversion from the amount of cement to that of clinker based on the cement/clinker ratio as in previous studies.^{4,6,16} The application rates of combustion/production techniques and APCDs were obtained from relevant industrial bulletins, previous studies, and expert consultation. The ULE retrofits were crucial APCD updates in China during 2015–2020. SI Section S4 briefly introduced the historical development and future prospect of ULE retrofits for key sectors. Desulfurization and denitrification devices for ULE retrofits with high Hg removal efficiencies were gradually applied in CFIBs, CCPs, and ISPs, which were also considered in this study. Details can be found in SI Tables S1–S4.^{4,6,15,16,22,24,35–38}

2.3.2. Hg Contents in Fuels and Raw Materials. Hg contents of the consumed fuels/raw materials were assumed to fit the lognormal distribution based on our previous study and relevant information from other studies.^{6,15,17,21,39–41} Hg contents of coals, non-ferrous metal concentrates, and limestones are listed in SI Tables S5–S6. Hg content in other raw materials used in CCP was 0.058 mg/kg as measured by Yang.³⁹ Interprovincial transport matrices for coal and metal concentrates (Zn, Pb, and Cu) were established based on consultation and previous studies.^{6,14,15}

2.3.3. Hg Removal Efficiencies of APCDs. The Hg removal efficiency of APCD is a crucial parameter for the estimation of Hg emission. Hg removal efficiencies of APCDs for NFMS were calculated considering the “removal compensation effect” of cascaded APCDs discussed in our previous study.¹⁵ For CFPP, Hg removal efficiencies of ESP, ESP+WFGD, and SCR+ESP+WFGD were calculated based on a coal quality-based submodel discussed in Section 2.2. Hg removal efficiencies for APCD combinations with enough test results were assumed to fit the Weibull distribution, while the remaining ones were assumed to fit the normal distribution.⁶ More detailed information can be found in SI Table S7.

The co-benefits of ULE retrofits in key sectors on Hg removal were discussed in detail in SI Section S4. SCR+ESP+FF/LTESP+WFGD and SCR+ESP+WFGD+WESP, which are the APCDs for ULE retrofits in the CFPP sector, enhanced the Hg removal efficiency to over 90%.⁴ Although SCR or selective noncatalytic reduction (SNCR) and ESP/FF were widespread in the CCP sector, Hg removal efficiencies for the commonly adopted precalciner process are much lower than the shaft/

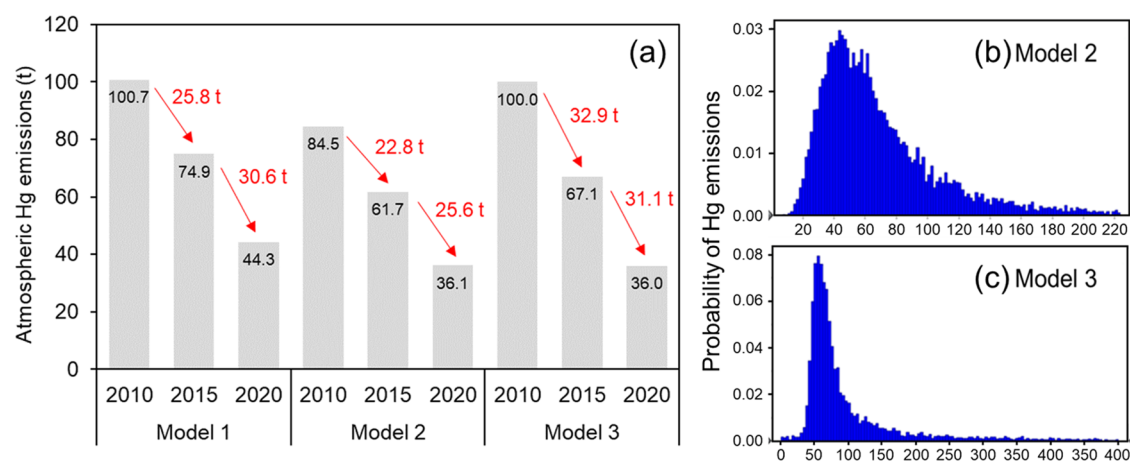


Figure 1. Comparison of Hg emissions from CFPPs based on three models (Model 1: deterministic technology-based model, Model 2: probabilistic technology-based model, Model 3: probabilistic technology-based model regarding the impact of coal quality on Hg removal efficiencies): (a) Hg emissions from CFPPs in China in 2010, 2015, and 2020; and the probability distributions of Hg emissions from CFPPs in 2015 based on (b) Model 2 and (c) Model 3.

rotary kiln process due to the existence of dust cycling.^{4,19} To meet the ULE standard, CCP has started to install WFGDs for SO₂ control which has high Hg removal efficiency, and ISP has started to install SCR for NO_x control which could enhance co-beneficial Hg removal efficiency in the downstream WFGDs. Since no on-site test results for these new APCD combinations are available so far, the Hg behavior inside these newly installed APCDs was estimated based on results from power plants.^{16,24}

2.3.4. Hg Speciation Profiles. The Hg speciation profile in exhausted flue gas depends on different APCD combinations equipped in Hg emission sources. Hg speciation profiles for most APCD combinations were mainly collected from previous studies.^{4,6,11,15,16,18} The ULE retrofits for the above-mentioned key sectors also have significant impacts on Hg speciation. The corona discharging inside WESP could form free radicals to oxidize part of Hg⁰ to Hg²⁺, and Hg²⁺ and Hg_p could be removed by WESP.³³ Hg²⁺ could also be adsorbed onto fly ash and removed in LTESP. As a result, the APCD combinations for ULE retrofit in CFPPs could lead to an increase in the percentage of Hg⁰.³³ Denitrification and desulfurization devices were installed in CFIBs, CCPs, and ISPs for ULE retrofit. For new APCD combinations, results from field measurements were prioritized. If no relevant results were available, the effects of similar APCD combinations in other sectors on Hg speciation profiles were considered, and the ultimate profiles were estimated. Detailed data are listed in SI Table S7.

2.4. Method for Developing Gridded Hg Emission Inventories. Hg emission sources were divided into point and non-point sources to develop the gridded emission maps. Hg emissions from point sources were calculated based on amounts of products manufactured or fuels consumed, production/combustion techniques adopted, and APCDs applied. The yields were directly put into the corresponding spatial grids based on their exact geographical coordinates, which were collected from relevant industrial associations. For non-point sources, provincial Hg emissions were allocated to the county level based on the gross domestic product (GDP) or the gross industrial product. Then, the county-level Hg emissions were interpolated to 27 km × 27 km gridded maps based on population data, road network data, and vegetation

distribution. Gridded Hg emission inventories for 2010, 2015, and 2020 were established.

2.5. Uncertainty Analysis. By taking the probability distributions of key parameters into consideration, Monte Carlo simulation was performed using the Crystal Ball software to analyze uncertainties of Hg emission inventories. The contributions of different factors to the overall uncertainty were obtained through the sensitivity analysis function of the software. The number of sampling was set to 10,000. The median value (P50) was considered as the best estimate, and the overall uncertainty of the emission was estimated based on a novel method developed in our previous study,⁶ which can be described by the following equation

$$u^{\pm} = \frac{Mo - \sqrt{\sigma_s^+ \sigma_k^+}}{P50} - 1 \quad (8)$$

where u is the uncertainty; Mo is the mode value; σ_s^- and σ_s^+ are the distances between Mo and the values, respectively, where the probability is equal to $f(Mo)/2$; and σ_k^- and σ_k^+ are the distances between Mo and P20 or P80, respectively.

3. RESULTS AND DISCUSSION

3.1. Improvements of Hg Emission Estimates for Key Sectors in China. Based on estimates from this study, CFPP, CFIB, NFMS, CCP, and ISP are the five key sectors in China, which have a significant overlap with the point source categories listed in Annex D of the Minamata Convention. The accuracies of Hg emission estimates for the five key sectors have all been improved significantly, leading toward more accurate effectiveness evaluation as addressed in Article 22 of the Minamata Convention.

The Hg emission estimates for CFPP and NFMS benefited mainly from the advancement in the submodels for Tier 4 methodology. Improvement for NFMS was embodied in the consideration of the “Hg removal compensation effect”, the details of which can be found in our previous study.¹⁵ The submodel for CFPP was built from our previous study.¹⁰ Hg behavior inside SCR was analyzed and quantified to improve the submodel. As shown in Figure 1, Hg emissions from CFPPs in China in 2010, 2015, and 2020 were calculated for comparison based on Tiers 2–4 models, which were named as

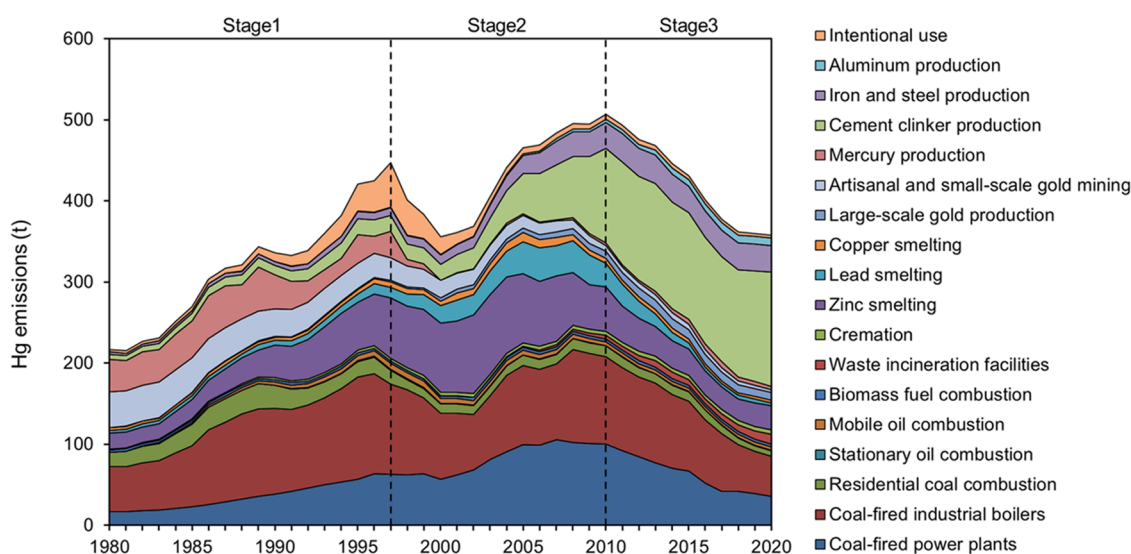


Figure 2. Anthropogenic Hg emissions in China by sector from 1980 to 2020.

Models 1–3, respectively. From Model 1 to 2, the Hg emission estimates in all three years decreased due to the skewed probability distribution of Hg content in coal. As a result, the amounts of Hg emission reduction during 2010–2015 and 2015–2020 with Model 2 were both lower than with Model 1. The Hg emission estimates in 2010 and 2015 with Model 3 were higher than with Model 2, which were mainly caused by the impacts of coal quality, especially Cl content, on Hg removal efficiencies in WFGD. As illustrated in our previous study,¹⁰ Cl content in coal plays an important role in the oxidation process of Hg^0 to Hg^{2+} , and the Hg removal efficiency of WFGD is proportional to the Hg^{2+} concentration in flue gas. Due to the low Cl content in raw coal in China, the outlet Hg^{2+} concentration of boilers in CFPPs is relatively low, leading to the lower Hg removal efficiencies of ESP+WFGD and SCR+ESP+WFGD (dominant combinations in 2010 and 2015). Hg emission estimate in 2020 with Model 3 was close to that with Model 2 because the combination of SCR+ESP+WFGD was largely replaced by the ULE combinations. Consequently, the amounts of Hg emission reduction during 2010–2015 and 2015–2020 were estimated to be 32.9 and 31.1 t by Model 3, which were 44.3 and 21.5% higher than those by Model 2, respectively. Moreover, the uncertainty of Model 3 was highly reduced (Figure 1b,c).

The Hg emission estimates for CFIB and CCP were improved mainly due to the update of activity level data from administration- or statistics-based to function- or technology-based. Coal used as fuel in cement kilns was regarded as industrial coal combustion in the CAME model⁶ due to the classification in energy statistical yearbooks in China for administrative purpose. However, this was not quite appropriate since the APCDs for CCPs and CFIBs were different. In the improved DIME model, this part of coal use was reclassified into the CCP sector, and the remaining coal consumption in the industrial sector excluding the use as raw materials was classified into the CFIB sector to address the point source category mentioned in the Minamata Convention. As a result, Hg emissions from CCP in 2010 estimated by the DIME model increased by 18 t compared to the CAME model⁶ while that from the CFIB sector decreased by 12 t, which provided a better estimate of Hg emissions from the sources of concern in the Minamata Convention.

The ULE retrofits contributed to significant Hg emission reduction during 2015–2020. For the CFPP sector, 46.1 t of Hg emission reduction was achieved from 2015 to 2020, with the installation rates of the combinations of SCR+ESP-FF/LTESP+WFGD and SCR+ESP+WFGD+WESP increased by 30 and 21%, respectively. The ULE retrofits for CFIB, ISP, and CCP have rarely been considered in previous studies. The overall Hg removal efficiency for the CFIB sector improved from 46% in 2017 to 61% in 2020 with the installation rates of WFGD and SCR increased by 31 and 10%, respectively, resulting in 15.9 t of Hg emission reduction from the CFIB sector during 2017–2020. The implementation of ULE retrofits in ISP and CCP took place in more recent years, especially SCR in ISPs and WFGD in CCPs. Hg emission reduction benefited from the updated APCDs in ISPs and CCPs during 2017–2020 were estimated to be 6.2 and 6.4 t, respectively. Although the Hg emission abatement from ULE retrofits for ISP and CCP was relatively modest, the potential of Hg emission reduction for the two sectors will be enormous in the near future.

3.2. Main Drivers for Trends in Anthropogenic Hg Emissions in China. Figure 2 and SI Figure S3 show the trends of anthropogenic Hg emissions in China by sector and of Hg emission speciation profiles, respectively, from 1980 to 2020. Based on the variation, historical Hg emissions can be divided into three stages as follows.

3.2.1. Stage 1: The Economy-Driven Rapid Growth Period (1980–1997). At this stage, the total anthropogenic Hg emissions in China increased rapidly from 217.0 t in 1980 to 447.1 t in 1997 with an average annual growth rate (AAGR) of 4.3%. The rapid economic growth in China in the 80s and 90s of the twentieth century was accompanied by industrial development and a sharp rise in electricity demand. Hg emissions from CFPPs, CFIBs, and Zn smelters increased by 45.6, 55.9, and 55.5 t, respectively. Moreover, Hg emissions from the intentional use sector increased by 52.4 t as incandescent lamps were widely replaced by fluorescent lamps which contain Hg to save electricity and economic costs. Artisanal and small-scale gold mining (ASGM) and Hg production were important emission sources as well at Stage 1, which contributed 11.8 and 11.9% to the total Hg emissions in 1997, respectively. This was caused by the high demand of

precious metals and the lack of control measures for artisanal and small-scale mining activities. The Hg emission speciation profile ($\text{Hg}^0/\text{Hg}^{2+}/\text{Hg}_p$) changed from 62.0/28.0/10.0 in 1980 to 58.3/33.3/8.7 in 1997, mainly due to the increasing Hg emissions from the NFMS sector with low pollution control level, 57% of which was Hg^{2+} in 1997. The proportion of Hg_p was relatively stable at this stage, while the proportion of Hg^0 experienced a slight increase during 1994–1997, resulting from the dramatic growth of Hg emissions from intentional use which was assumed to emit 100% Hg^0 .

3.2.2. Stage 2: The Growth-Control Offsetting Period (1997–2010). With the impact of the Asian financial crisis in 1998, the national Hg emissions in China decreased sharply to 355.6 t in 2000. The fast reduction of activity levels (>65%) of intentional use contributed to over 30% Hg emission reduction during 1997–2000. In 1997, Regulation on Limiting the Amount of Mercury in Battery Products was issued to explicitly prohibit the sale of Hg-containing batteries by 2006. Therefore, Hg emissions from the intentional use sector decreased significantly due to the replacement of non-Hg products. Emission reduction from Hg mining could be attributed to the decline of demand for primary Hg and the increase in the use of recycled Hg. Due to the significant influence of the crisis on the activity level of coal combustion, 30.6 t Hg emission reduction occurred to CFIBs, while the growth of Hg emissions from CFPPs stopped. After 2000, the economy in China started to recover and accelerate again. During the first decade of this century, the activity levels of all key sectors, including CFPP, CFIB, NFMS, CCP, and ISP experienced rapid growth. However, the offsetting effect brought by air pollution control measures in these sectors limited the growth of Hg emissions in China (to 506.6 t in 2010). PM control devices in all of these sectors were the pioneers in the abatement of Hg emissions, although the Hg removal efficiencies of wet scrubber (WS) and ESP are not very high. The high SO_2 concentrations in flue gases in the NFMS sector can be used to produce sulfuric acid to obtain economic benefits. As a result, the popularization of acid plants with the double-contact-double-absorption (DCDA) process and the elimination of small-scale smelters since 2003 made NFMS the biggest Hg emission control sector, especially Zn smelting with 30.5 t Hg emission reduction during 2000–2010.

Hg emissions from ASGM gradually declined resulting from the prohibition of artisanal gold mining by the Mine Eco-Environmental Protection and Pollution Control Technology Policies released in 2005. With the strict control measures for SO_2 in the 11th Five-Year Plan (2005–2010), WFGDs with high Hg removal efficiencies were installed extensively in CFPPs in China. The only exception was CCP, which turned out to be the main driver of Hg emission growth at Stage 2. The Cement Industry Development Policy issued in 2006 vigorously promoted the new dry-process precalciner technique due to its high efficiency, good quality, and low energy demand. Consequently, the application rate of the new dry-process precalciner technique in CCPs increased sharply from about 10% in 2000 to 82% in 2010, leading to extremely low Hg removal efficiency (6.2%) due to dust cycling in kiln systems. As a result, Hg emissions from CCP boosted from 19.3 t in 2000 to 116.4 t in 2010 and became the biggest Hg emission sector in China. The Hg emission speciation profile ($\text{Hg}^0/\text{Hg}^{2+}/\text{Hg}_p$) changed greatly to 54.0/43.2/2.8 in 2010. Due to the popularization of dust removal devices, the

proportion of Hg_p decreased rapidly. The proportion of Hg^0 experienced another slight increase during 2005–2008 due to the widespread application of WFGD in CFPPs which removes a large amount of Hg^{2+} .

3.2.3. Stage 3: The Economy-Decoupled Fast Declining Period (2010–2020). At this stage, the total anthropogenic Hg emission decreased from 506.6 t in 2010 to 357.8 t in 2020 with an AAGR of –3.4%, mainly due to Hg emission control in NFMSs, CFPPs, and CFIBs. With the implementation of the Minamata Convention, China continued to strengthen the replacement of Hg-containing products. Ministry of Ecology and Environment of China announced that fluorescent lamps and Hg-containing batteries will no longer be used by 2021, and production of Hg-containing thermometers and sphygmomanometers will stop completely by 2026. Due to the elimination of the outdated sintering machine process (SMP) and sintering pan/pot process (SPP) and the updated APCD combinations, Pb smelting contributed 26.1 t Hg emission reduction. Zn smelting contributed 25.0 t emission reduction, which was mainly benefited from the enhanced SO_2 control technologies (the installation rate of WFGD reached 47% in 2020). The Hg emissions from CFPPs continued to decline with the installation of SCR (from 12.0 to 85.3%) as the main driver during 2010–2015, and with the application of ULE retrofit as the main driver (resulting in 46.1 t Hg emission reduction) during 2015–2020.

With the implementation of Air Pollution Prevention and Control Action Plan during 2013–2017, Hg emissions decreased by 91.0 t, with 35.0, 27.1, and 22.8 t of Hg emission reduction from the CFPP, CFIB, and NFMS sectors, respectively. Hg emission from CCP experienced a slight decrease during this period due to the widespread installation of SNCR+ESP/FF. With the implementation of the Three-year Action Plan for Winning the Blue Sky Battle, the CFIB sector was the largest Hg emission reduction sector from 2017 to 2020 (by 21.8 t), mainly resulting from the replacement of ESP with FF and the newly installed desulfurization and denitrification devices. The action plan also triggered the installation of WFGD in the CCP sector. However, the sharp growth of cement clinker production offset the Hg emission reduction by the limited application of the updated APCD combination (<10%). The total Hg emission reduction during 2017–2020 was only 19.7 t because Hg emissions from CCP increased to 141.2 t in 2020 with the thorough adoption of the precalciner technology. The potential of Hg emission abatement is still high for CCP. At this stage, the proportion of Hg^0 experienced a third slight increase during 2015–2017, not only resulting from the ULE retrofit in CFPPs but also due to the massive installation of SNCR in CCPs and DFGD in NFMSs, which had very limited Hg removal efficiencies but could turn Hg^{2+} to Hg^0 . The decline of the Hg^0 proportion after 2017 was mainly due to the increase of the combination of DC+FGS+ESD+DCDA+WFGD in Zn smelting. Consequently, the overall Hg emission speciation profile ($\text{Hg}^0/\text{Hg}^{2+}/\text{Hg}_p$) changed to 53.1/44.3/2.6 in 2020.

3.3. Main Drivers for Changes in Spatial Distributions of Hg Emissions in China. Gridded anthropogenic Hg emissions in China in 2010, 2015, and 2020 are shown in Figure 3. Hg emissions were mainly concentrated in the North China Plain (NCP), the Yangtze River Delta (YRD), the Pearl River Delta (PRD), central China, and southwest China, which accounted for over 70% of national Hg emissions. Changes in the spatial distribution of Hg emissions in China are shown in

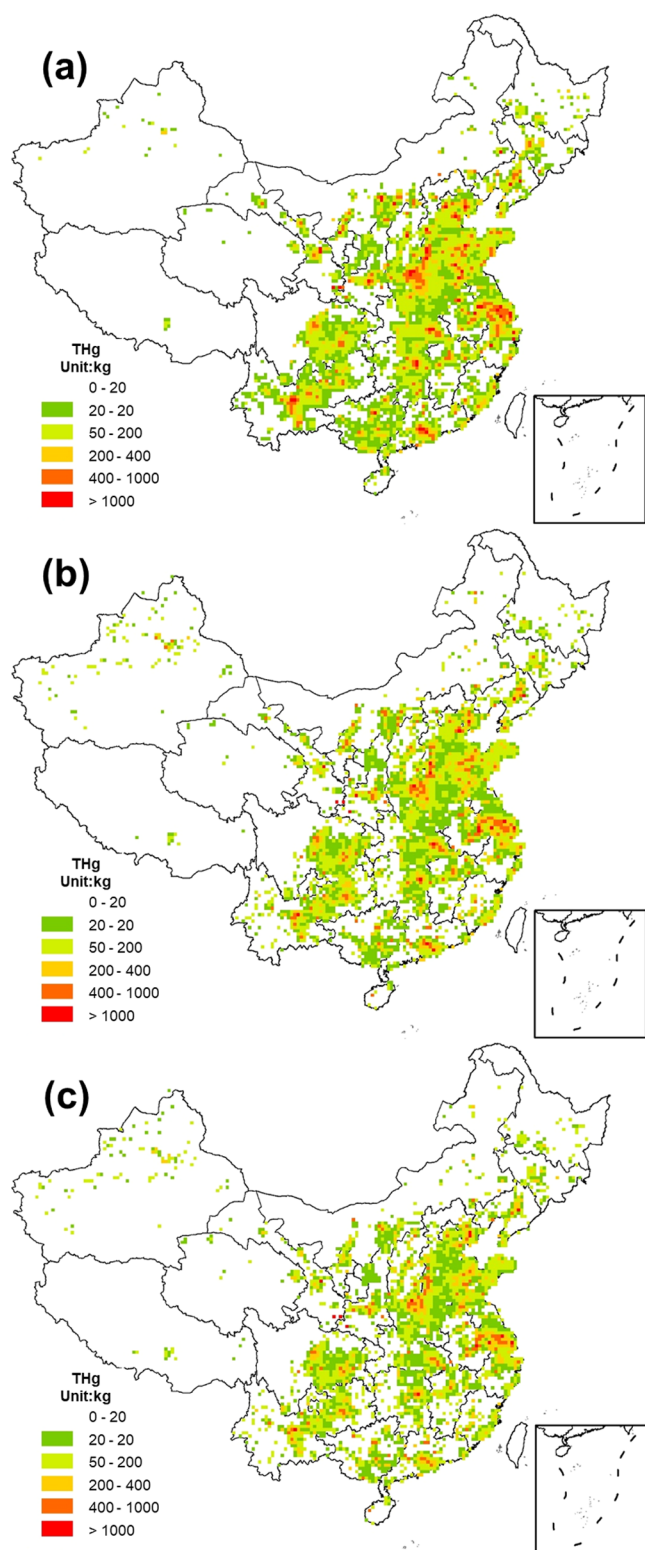


Figure 3. Gridded total anthropogenic Hg emissions in China in (a) 2010, (b) 2015, and (c) 2020.

Figure 4. From 2010 to 2015, the top three provinces with the biggest Hg emission reduction were Henan, Gansu, and Shandong, which accounted for 47.1% of the national emission reduction. Henan was still the biggest Hg emitter in 2015, although the Hg emission reduction was as much as 14.1 t with CFIB and NFMS as the main contributing sectors. Due to the upgrading APCDs and the elimination of outdated lead

smelting technologies, Pb smelting contributed 8.5 t emission reduction in Henan. With the implementation of the Overall Plan of Circular Economy, Gansu was the province with the largest Hg emission reduction from the NFMS sector, and almost all of Hg emission reduction in Gansu came from Zn smelting (12.5 t), mainly resulting from the installation of WFGD. The Hg emission reduction in the regions of NCP, YRD, PRD, and southwest China was mainly benefited from the enhanced SO_2 and NO_x control in CFPPs and CFIBs. The NFMS sector contributed to additional Hg emission reduction in southwest China. Due to the continuous growth of domestic infrastructure needs, the capacity of CCP has increased sharply since 2010. The increase of Hg emissions caused by CCPs with rapid growth of clinker production and application of the precalciner technology was mainly concentrated in Henan (5.2 t) and southwest China (4.4 t). Hg emissions reduction from 2010 to 2015 was mainly Hg^0 due to Hg emission reduction from CFPPs and CFIBs, as shown in SI Figure S4. Due to the gradual tightening of air pollution emission standards in various regions, Hg emission abatement was mainly concentrated in urban area where more industrial pollution was generated and controlled.

From 2015 to 2020, eastern and central China had the largest reduction of Hg emissions. Although activity levels of most sectors continued to rise, Hg emissions were still decreasing in most regions due to the application of more stringent local emission standards, especially the special emission limits for key regions, such as NCP, YRD, and PRD. With the ULE retrofits in eastern China, 13.1 t from CFPPs and 10.5 t from CFIBs were abated. The APCD combinations for ULE, i.e., SCR+ESP-FF/LTESP+WFGD and SCR+ESP+WFGD+WESP, reached over 70% in CFPPs in 2020. For CFIBs, the desulfurization and denitrification devices increased by 45 and 12% from 2015 to 2020, respectively. Due to the capacity reduction requirements in the Structural Adjustment Plan of Cement Industry in Henan issued in 2014, the amount of clinker production in Henan decreased by 21%. As a result, Hg emissions from CCPs in Henan reduced 5.8 t, which contributed to 37% of Hg emission reduction in central China. The total Hg emission in Hebei increased by 2.5 t with 61% increase in clinker production. Moreover, the increase in Hg emissions in some provinces with large populations (such as Shandong and Henan) also originated from WIFs due to its rapidly increasing activity levels. SNCR widely installed in CCPs changed the Hg emission speciation profile ($\text{Hg}^0/\text{Hg}^{2+}/\text{Hg}_p$) of the CCP sector from 33.6/65.4/1.0 in 2015 to 48.2/50.8/1.0 in 2020. With the gradual development of ULE retrofit in CCPs, WFGD will be widely installed in the future, which can lead to the rise of the proportion of Hg^{2+} . The distribution of point sources for CFPPs, NFMSs, CCPs, and ISPs in 2020 were shown in SI Figure S5. The CCP sector emitted 71.8 t Hg^{2+} in 2020 and contributed over 46% to the total Hg^{2+} emissions in China, which could cause a large amount of Hg deposition nearby especially in eastern and central China, resulting in higher risk of Hg exposure in these areas.

3.4. Comparison with Previous Inventories. A comparison of the total national Hg emissions between this study and previous studies is shown in Figure 5.^{4,6,12,25,27,42,43} Mainly due to the ignored high Hg removal efficiencies of acid plants in NFMSs,^{41,44} Hg emissions in 2000 estimated by Wu et al.¹² were much higher than the results from this study. Hg emissions in 2005 and 2010 estimated by Zhao et al.²⁷ were 46

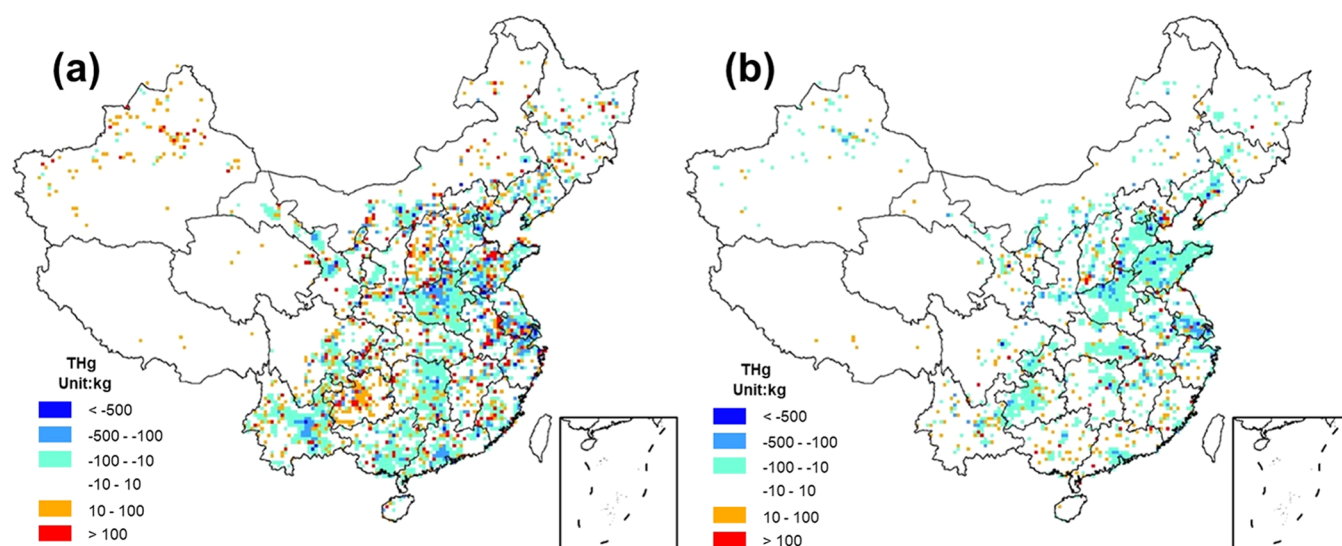


Figure 4. Changes in spatial distributions of Hg emissions in China: (a) from 2010 to 2015; (b) from 2015 to 2020.

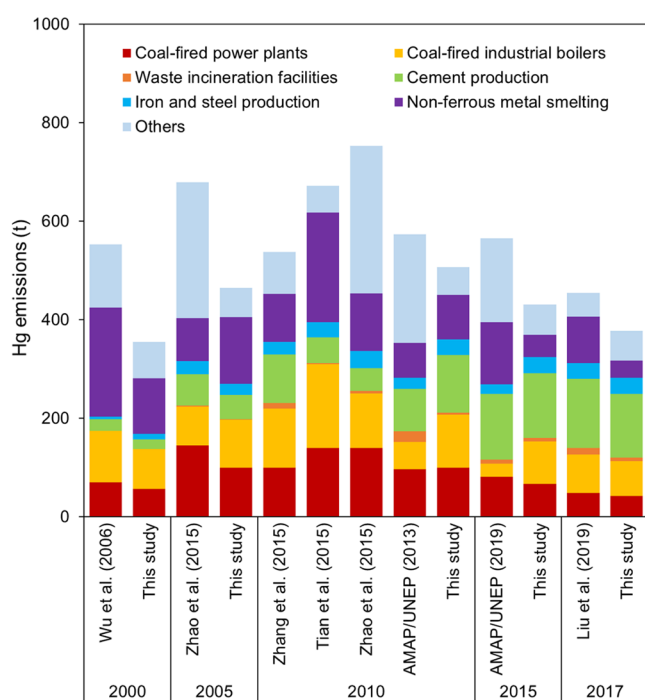


Figure 5. Comparison of the total national Hg emissions between previous studies and this study.

and 49% higher than the estimates from this study, respectively, which was mainly due to the large sectoral emission estimate from ASGM (166.7 t). It was inherited from previous studies^{27,43} and proven unreasonable due to China's ban on ASGM.⁶ The slight discrepancy of Hg emissions in 2010 estimated by this study and our previous study⁶ was caused by the reclassification of coal combustion. The differences between this study and the Global Mercury Assessment reports^{42,43} were the most significant due to inconsistency of methodology and activity levels, especially for the sectors of ASGM, CFIB, NFMS, and intentional use. The Hg removal compensation effect in the NFMS sector discovered in our previous study¹⁵ was the main cause for the discrepancy between this study and Liu et al.⁴ in Hg emission estimates for recent years.

The overall uncertainty ranges (equivalent to $\pm\sigma$) for the anthropogenic Hg emission estimates in this study varied from (−32%, 38%) in 1980 to (−18%, 23%) in 2020, as shown in SI Figure S7. The estimates by Zhang et al.⁶ and Wu et al.¹⁸ were basically within the uncertainty ranges of this study. The EDGAR emission estimates⁴⁵ were within the uncertainty ranges of this study for the first decade of this century but could be biased low for 1980–2000 due to the underestimation of activity levels. Uncertainty ranges of previous studies were listed in SI Table S9. Although there were inconsistencies in the confidence interval, the uncertainty range in this study was still at a low level among the existing studies. More importantly, the significant estimate biases for NFMS and ASGM could weaken the reliability of the uncertainty ranges given by Wu et al.,¹² Tian et al.,²⁵ and Zhao et al.²⁷ As shown in SI Figure S8, the significant decrease of the overall uncertainty in this study was mainly benefited from the advanced Hg emission estimation submodels and the updated information on Hg contents of fuels/raw materials and Hg removal efficiencies of APCDs. The uncertainties for the sectors of CFPP, CFIB, NFMS, CCP, and ISP in 2020 were calculated to be (−31%, 34%), (−42%, 40%), (−28%, 30%), (−31%, 51%), and (−29%, 77%), respectively. The Hg contents in coals produced from Inner Mongolia and Shaanxi, the two largest coal production provinces in China, contributed 44.2 and 22.9% to the uncertainty of Hg emissions from CFPP, respectively, and 49.6 and 23.0% to that for CFIB. For NFMS, Hg contents in metal concentrates were the biggest contributors to the overall uncertainty of Hg emissions, the remaining uncertainty contributions came from activity levels and Hg removal efficiencies of APCDs. Since Hg emissions from CCP included coal use as fuel, the main source of uncertainty for CCP was the Hg contents in coals, which exceeded 80%. The Hg content in limestone produced from Hubei contributed 11.4% to the overall uncertainty of Hg emissions from CCP.

4. IMPLICATIONS AND LIMITATIONS

Effectiveness evaluation for the implementation of the Minamata Convention on Mercury includes accurate estimation of emission reduction and pollution alleviation, with the latter simulated based on chemical transport models (CTMs).

The accuracy of Hg emission reduction estimation is mainly related to the improvement of the inventory models for key sources and the consistency of historical emission calculation. In this study, the DIME model was developed for estimating anthropogenic Hg emissions in China. The more advanced submodels in this study for NFMS and CFPP regarding the Hg behaviors inside APCDs and the more updated information on Hg removal efficiencies for comprehensive APCD combinations for ULE retrofits have improved the accuracy and reliability of Hg emission estimates for key sectors, which could benefit Hg emission reduction evaluation. The consistency of methodology in estimating historical inventories for 40 years is another highlight of this study. With more accurate Hg emission estimates and point source information, the gridded Hg emission inventories for 2010, 2015, and 2020 established in this study could contribute to more accurate spatial distribution and Hg speciation profiles, which will be conducive to the simulation of CTMs in the future. With the continuous promotion of ULE retrofits, especially for the CCP sector, the potential of Hg emission reduction will be further released. Moreover, under the goal of carbon neutrality in China, the transformation of energy structure and industrial structure will also bring about large Hg emission reduction in the future.

The limitation of this study lies in two aspects, the lack of field measurements for more advanced APCD combinations and the simplification of emission estimation methods for rapidly developing sectors (e.g., WIF). Therefore, more field tests on the APCD combinations for ULE retrofits should be carried out to develop more refined submodels and obtain more reliable Hg removal efficiencies, such as SCR+ESP-FF+WFGD+WESP in CFPPs and the APCD combinations about to be widely installed in CCPs and ISPs. Due to the large variation range of Hg contents in solid wastes for WIFs, the contribution of its uncertainty to the overall uncertainty could increase significantly with the fast development of this sector. Method improvements for sectors like WIF are in urgent need, such as the life cycle assessment (LCA) approach to track the holistic Hg flow.

■ ASSOCIATED CONTENT

Data Availability Statement

Data will be made available upon request.

SI Supporting Information

The Supporting Information is available free of charge at <https://pubs.acs.org/doi/10.1021/acs.est.3c01065>.

Description of methods for the four tiers of emission sources; submodels for the calculation of Hg emissions from CFPPs; reclassification for coal use in the DIME model; key parameters used in DIME model; changes in spatial distributions of speciated Hg emissions; spatial distribution of point sources and speciated Hg emissions; and results from uncertainty analysis (PDF)

■ AUTHOR INFORMATION

Corresponding Author

Lei Zhang – School of the Environment, and State Key Laboratory of Pollution Control and Resource Reuse, Nanjing University, Nanjing, Jiangsu 210023, China; Jiangsu Collaborative Innovation Center of Atmospheric Environment and Equipment Technology, Nanjing University of Information Science and Technology, Nanjing, Jiangsu

210044, China; orcid.org/0000-0003-2796-6043;
Email: lzhang12@nju.edu.cn

Authors

Yang Zhang – School of the Environment, and State Key Laboratory of Pollution Control and Resource Reuse, Nanjing University, Nanjing, Jiangsu 210023, China

Shuzhen Cao – School of the Environment, and State Key Laboratory of Pollution Control and Resource Reuse, Nanjing University, Nanjing, Jiangsu 210023, China

Xia Liu – School of the Environment, and State Key Laboratory of Pollution Control and Resource Reuse, Nanjing University, Nanjing, Jiangsu 210023, China

Jingmeng Jin – School of the Environment, and State Key Laboratory of Pollution Control and Resource Reuse, Nanjing University, Nanjing, Jiangsu 210023, China

Yu Zhao – School of the Environment, and State Key Laboratory of Pollution Control and Resource Reuse, Nanjing University, Nanjing, Jiangsu 210023, China; Jiangsu Collaborative Innovation Center of Atmospheric Environment and Equipment Technology, Nanjing University of Information Science and Technology, Nanjing, Jiangsu 210044, China

Complete contact information is available at:

<https://pubs.acs.org/10.1021/acs.est.3c01065>

Notes

The authors declare no competing financial interest.

■ ACKNOWLEDGMENTS

This work was funded by the National Natural Science Foundation of China (no. 42277079 and no. 21876077) and the Natural Resources Defense Council (NRDC). The authors thank Prof. Shuxiao Wang and Dr. Long Wang for their help on emission inventory development, and Mr. Zhuqiang Shao and Mr. Fengzhou Yue for their valuable consultation.

■ REFERENCES

- (1) Zhang, L.; Wang, S.; Wu, Q.; Wang, F.; Lin, C.-J.; Zhang, L.; Hui, M.; Yang, M.; Su, H.; Hao, J. Mercury transformation and speciation in flue gases from anthropogenic emission sources: a critical review. *Atmos. Chem. Phys.* **2016**, *16*, 2417–2433.
- (2) Obrist, D.; Kirk, J. L.; Zhang, L.; Sunderland, E. M.; Jiskra, M.; Selin, N. E. A review of global environmental mercury processes in response to human and natural perturbations: Changes of emissions, climate, and land use. *Ambio* **2018**, *47*, 116–140.
- (3) Bai, X.; Tian, H.; Zhu, C.; Luo, L.; Hao, Y.; Liu, S.; Guo, Z.; Lv, Y.; Chen, D.; Chu, B.; Wang, S.; Hao, J. Present Knowledge and Future Perspectives of Atmospheric Emission Inventories of Toxic Trace Elements: A Critical Review. *Environ. Sci. Technol.* **2023**, *57*, 1551–1567.
- (4) Liu, K.; Wu, Q.; Wang, L.; Wang, S.; Liu, T.; Ding, D.; Tang, Y.; Li, G.; Tian, H.; Duan, L.; Wang, X.; Fu, X.; Feng, X.; Hao, J. Measure-Specific Effectiveness of Air Pollution Control on China's Atmospheric Mercury Concentration and Deposition during 2013–2017. *Environ. Sci. Technol.* **2019**, *53*, 8938–8946.
- (5) Wu, Q.; Wang, S.; Liu, K.; Li, G.; Hao, J. Emission-Limit-Oriented Strategy To Control Atmospheric Mercury Emissions in Coal-Fired Power Plants toward the Implementation of the Minamata Convention. *Environ. Sci. Technol.* **2018**, *52*, 11087–11093.
- (6) Zhang, L.; Wang, S. X.; Wang, L.; Wu, Y.; Duan, L.; Wu, Q. R.; Wang, F. Y.; Yang, M.; Yang, H.; Hao, J. M.; Liu, X. Updated emission inventories for speciated atmospheric mercury from anthropogenic sources in China. *Environ. Sci. Technol.* **2015**, *49*, 3185–3194.

- (7) Tong, Y.; Gao, J.; Wang, K.; Jing, H.; Wang, C.; Zhang, X.; Liu, J.; Yue, T.; Wang, X.; Xing, Y. Highly-resolved spatial-temporal variations of air pollutants from Chinese industrial boilers. *Environ. Pollut.* **2021**, *289*, No. 117931.
- (8) Streets, D.; Hao, J.; Wu, Y.; Jiang, J.; Chan, M.; Tian, H.; Feng, X. Anthropogenic mercury emissions in China. *Atmos. Environ.* **2005**, *39*, 7789–7806.
- (9) Wang, S. X.; Zhang, L.; Li, G.; Wu, Y.; Hao, J.; Pirrone, N.; Sprovieri, F.; Ancora, M. P. Mercury emission and speciation of coal-fired power plants in China. *Atmos. Chem. Phys.* **2010**, *10*, 1183–1192.
- (10) Zhang, L.; Wang, S.; Meng, Y.; Hao, J. Influence of Mercury and Chlorine Content of Coal on Mercury Emissions from Coal-Fired Power Plants in China. *Environ. Sci. Technol.* **2012**, *46*, 6385–6392.
- (11) Liu, K.; Wang, S.; Wu, Q.; Wang, L.; Ma, Q.; Zhang, L.; Li, G.; Tian, H.; Duan, L.; Hao, J. A Highly Resolved Mercury Emission Inventory of Chinese Coal-Fired Power Plants. *Environ. Sci. Technol.* **2018**, *52*, 2400–2408.
- (12) Wu, Y.; Wang, S.; Streets, D. G.; Hao, J.; Chan, M.; Jiang, J. Trends in anthropogenic mercury emissions in China from 1995 to 2003. *Environ. Sci. Technol.* **2006**, *40*, 5312–5318.
- (13) Hylander, L. D.; Herbert, R. B. Global emission and production of mercury during the pyrometallurgical extraction of nonferrous sulfide ores. *Environ. Sci. Technol.* **2008**, *42*, 5971–5977.
- (14) Wu, Q. R.; Wang, S.; Zhang, L.; Song, J.; Yang, H.; Meng, Y. Update of mercury emissions from China's primary zinc, lead and copper smelters, 2000–2010. *Atmos. Chem. Phys.* **2012**, *12*, 11153–11163.
- (15) Cao, S.; Zhang, L.; Zhang, Y.; Wang, S.; Wu, Q. Impacts of Removal Compensation Effect on the Mercury Emission Inventories for Nonferrous Metal (Zinc, Lead, and Copper) Smelting in China. *Environ. Sci. Technol.* **2022**, *56*, 2163–2171.
- (16) Wu, Q.; Li, G.; Wang, S.; Liu, K.; Hao, J. Mitigation Options of Atmospheric Hg Emissions in China. *Environ. Sci. Technol.* **2018**, *52*, 12368–12375.
- (17) Chen, L.; Liang, S.; Zhang, H.; Cai, X.; Chen, Y.; Liu, M.; Lin, H.; Li, Y.; Qi, J.; Tong, Y.; Zhang, W.; Wang, X.; Shu, J. Rapid Increase in Cement-Related Mercury Emissions and Deposition in China during 2005–2015. *Environ. Sci. Technol.* **2020**, *54*, 14204–14214.
- (18) Wu, Q.; Wang, S.; Li, G.; Liang, S.; Lin, C. J.; Wang, Y.; Cai, S.; Liu, K.; Hao, J. Temporal Trend and Spatial Distribution of Speciated Atmospheric Mercury Emissions in China During 1978–2014. *Environ. Sci. Technol.* **2016**, *50*, 13428–13435.
- (19) Wang, F.; Wang, S.; Zhang, L.; Yang, H.; Wu, Q.; Hao, J. Mercury enrichment and its effects on atmospheric emissions in cement plants of China. *Atmos. Environ.* **2014**, *92*, 421–428.
- (20) Li, Z.; Huang, Y.; Liu, J.; Sun, G.; Wang, Q.; Xiao, H.; Huang, M. Mass flow, enrichment and potential environmental impacts of mercury in a preheater-precalciner cement plant using multiple mining and industrial wastes. *J. Environ. Manage.* **2022**, *311*, No. 114819.
- (21) Cai, X.; Cai, B.; Zhang, H.; Chen, L.; Zheng, C.; Tong, P.; Lin, H.; Zhang, Q.; Liu, M.; Tong, Y.; Wang, X. Establishment of High-Resolution Atmospheric Mercury Emission Inventories for Chinese Cement Plants Based on the Mass Balance Method. *Environ. Sci. Technol.* **2020**, *54*, 13399–13408.
- (22) National Energy Statistical Agency of China (NESA). *China Energy Statistical Yearbook*; NESA: Beijing, China, 1986–2021.
- (23) Tong, Y.; Wang, K.; Gao, J.; Yue, T.; Zuo, P.; Wang, C.; Tong, L.; Zhang, X.; Zhang, Y.; Liang, Q.; Liu, J. Mercury distribution and emission reduction potentials of Chinese coal-fired industrial boilers. *Air Qual. Atmos. Health* **2022**, *15*, 967–978.
- (24) Wu, Q.; Gao, W.; Wang, S.; Hao, J. Updated atmospheric speciated mercury emissions from iron and steel production in China during 2000–2015. *Atmos. Chem. Phys.* **2017**, *17*, 10423–10433.
- (25) Tian, H. Z.; Zhu, C.-Y.; Gao, J. J.; Cheng, K.; Hao, J. M.; Wang, K.; Hua, S. B.; Wang, Y.; Zhou, J. R. Quantitative assessment of atmospheric emissions of toxic heavy metals from anthropogenic sources in China: historical trend, spatial distribution, uncertainties, and control policies. *Atmos. Chem. Phys.* **2015**, *15*, 10127–10147.
- (26) Huang, Y.; Deng, M.; Li, T.; Japenga, J.; Chen, Q.; Yang, X.; He, Z. Anthropogenic mercury emissions from 1980 to 2012 in China. *Environ. Pollut.* **2017**, *226*, 230–239.
- (27) Zhao, Y.; Zhong, H.; Zhang, J.; Nielsen, C. P. Evaluating the effects of China's pollution controls on inter-annual trends and uncertainties of atmospheric mercury emissions. *Atmos. Chem. Phys.* **2015**, *15*, 4317–4337.
- (28) Wang, K.; Tong, Y.; Yue, T.; Gao, J.; Wang, C.; Zuo, P.; Liu, J. Measure-specific environmental benefits of air pollution control for coal-fired industrial boilers in China from 2015 to 2017. *Environ. Pollut.* **2021**, *273*, No. 116470.
- (29) Hu, Y.; Cheng, H.; Tao, S. The growing importance of waste-to-energy (WTE) incineration in China's anthropogenic mercury emissions: Emission inventories and reduction strategies. *Renew. Sustainable Energy Rev.* **2018**, *97*, 119–137.
- (30) Zhao, S.; Duan, Y.; Yao, T.; Liu, M.; Lu, J.; Tan, H.; Wang, X.; Wu, L. Study on the mercury emission and transformation in an ultra-low emission coal-fired power plant. *Fuel* **2017**, *199*, 653–661.
- (31) Pudasainee, D.; Kim, J.-H.; Yoon, Y.-S.; Seo, Y.-C. Oxidation, reemission and mass distribution of mercury in bituminous coal-fired power plants with SCR, CS-ESP and wet FGD. *Fuel* **2012**, *93*, 312–318.
- (32) Pudasainee, D.; Seo, Y.-C.; Sung, J.-H.; Jang, H.-N.; Gupta, R. Mercury co-beneficial capture in air pollution control devices of coal-fired power plants. *Int. J. Coal Geol.* **2017**, *170*, 48–53.
- (33) Zhang, Y.; Yang, J.; Yu, X.; Sun, P.; Zhao, Y.; Zhang, J.; Chen, G.; Yao, H.; Zheng, C. Migration and emission characteristics of Hg in coal-fired power plant of China with ultra low emission air pollution control devices. *Fuel Process. Technol.* **2017**, *158*, 272–280.
- (34) Zhou, Z.-J.; Liu, X.; Zhao, B.; Chen, Z.; Shao, H.; Wang, L.; Xu, M. Effects of existing energy saving and air pollution control devices on mercury removal in coal-fired power plants. *Fuel Process. Technol.* **2015**, *131*, 99–108.
- (35) Nonferrous Metal Industry Association of China (NMIA). *Yearbook of Nonferrous Metals Industry of China*; NMIA: Beijing, China, 1991–2019.
- (36) Liao, S.; Wang, D.; Xia, C.; Tang, J. China's provincial process CO₂ emissions from cement production during 1993–2019. *Sci. Data* **2022**, *9*, No. 165.
- (37) National Statistical Bureau of China (NSB). *China Industry Statistical Yearbook*; NSB: Beijing, China, 1986–2021.
- (38) National Statistical Bureau of China (NSB). *China Statistical Yearbook*; NSB: Beijing, China, 1981–2021.
- (39) Yang, H. Study on Atmospheric Mercury Emission and Control Strategies from Cement Production in China; M.S. thesis; Tsinghua University: Beijing, China, 2014.
- (40) Zhang, L. Emission Characteristics and Synergistic Control Strategies of Atmospheric Mercury from Coal Combustion in China; Ph.D. thesis; Tsinghua University: Beijing, China, 2012.
- (41) Wu, Q. Characteristics and abatement potential of mercury emission for China's nonferrous metal smelting industries; Ph.D. thesis; Tsinghua University: Beijing, China, 2015.
- (42) Arctic Monitoring and Assessment Programme (AMAP) and United Nations Environment Programme (UNEP). *Technical Background Report to the Global Mercury Assessment 2018*; UNEP Chemicals Branch: Geneva, Switzerland, 2019.
- (43) Arctic Monitoring and Assessment Programme (AMAP) and United Nations Environment Programme (UNEP). *Technical Background Report to the Global Mercury Assessment 2013*; UNEP Chemicals Branch: Geneva, Switzerland, 2013.
- (44) Zhang, L.; Wang, S.; Wu, Q.; Meng, Y.; Yang, H.; Wang, F.; Hao, J. Were mercury emission factors for Chinese non-ferrous metal smelters overestimated? Evidence from onsite measurements in six smelters. *Environ. Pollut.* **2012**, *171*, 109–117.
- (45) Muntean, M.; Janssens-Maenhout, G.; Song, S.; Giang, A.; Selin, N. E.; Zhong, H.; Zhao, Y.; Olivier, J. G. J.; Guizzardi, D.; Crippa, M.; Schaaf, E.; Dentener, F. Evaluating EDGARv4.tox2

speciated mercury emissions ex-post scenarios and their impacts on modelled global and regional wet deposition patterns. *Atmos. Environ.* 2018, 184, 56–68.